Serb. Astron. J. № 211 (2025), 45 - 57 UDC 523.345 : 52–421.4 : 528.8
DOI: https://doi.org/10.2298/SAJ2511045U Original scientific paper

UPDATED RADIO $\Sigma - D$ RELATION AND DISTANCES TO THE SHELL-LIKE GALACTIC SUPERNOVA REMNANTS - IV

D. Urošević[1], B. Vukotić[2], M. Andjelić[1] and N. Mladenović[2]

[1] *Department of Astronomy, Faculty of Mathematics, University of Belgrade Studentski trg 16, 11000 Belgrade, Serbia*

E–mail: *dejanu@math.rs*

[2] *Astronomical Observatory, Volgina 7, 11060 Belgrade 38, Serbia*

(Received: June 30, 2025; Accepted: September 2, 2025)

SUMMARY: We present a new selected sample of 69 Galactic supernova remnants (SNRs) for calibration of the radio $\Sigma - D$ relation at 1 GHz. Calibrators with the most reliable distances were selected through an extensive literature search. The calibration is performed using kernel smoothing of the chosen sample of calibrators in the $\Sigma - D$ plane and an orthogonal offsets fitting procedure. We use the obtained calibration to derive the distances to 164 Galactic SNRs and 27 new detected SNRs/SNR candidates with none or poor distance estimates. The analysis given in this paper confirms the expected predictions from our previous papers that the kernel smoothing method is more reliable for SNR distance calibration than the orthogonal offset fitting method, except for the distance determinations of the very low brightness SNRs.

Key words. Methods: data analysis – Methods: statistical – Astronomical data bases: miscellaneous – ISM: supernova remnants – Radio continuum: ISM

1. INTRODUCTION

A relation between radio surface brightness (Σ) at frequency ν and diameter (D) of an expanding spherical shell-like supernova remnant (SNR) was proposed by Shklovskii (1960):

$$\Sigma_\nu = AD^\beta, \tag{1}$$

with exponent β dependent on a spectral index α, that characterizes the flux density distribution of radio-emission as $S_\nu \propto \nu^{-\alpha}$, and on change of the magnetic field strength through the SNR evolution. A parameter A characterizes properties of a supernova explosion coupled with the density and magnetic field strength of the SNR environment.

SNRs are strong emitters of radio synchrotron radiation. At present, there are ≈ 310 SNRs detected in the Milky Way (Green 2025). The majority (92%) of the 310 Galactic SNRs are detected at radio frequencies, while ≈ 46% of them are detected at X-ray, and ≈ 32% at optical wavelengths (Green 2025). Because of observational constraints and selection effects, there is an apparent deficit of the observed number of Galactic SNRs. By using two different methods, Ranasinghe and Leahy (2022) derived that there should be between 2400 − 5600 SNRs in our Galaxy. While the predicted number of SNRs for the Galaxy is a few thousand, the observations/detections of the new SNRs could be limited to a few hundred. With the golden era of radio astronomy at our doorstep (for some of the recent SNR discoveries see Sasaki et al. 2025, Filipović et al. 2024, Smeaton et al. 2024b), the number of radio SNRs should be significantly increased.

Distances to these objects can be determined using various methods, but they often require observations across the entire electromagnetic spectrum. When only the radio flux of an SNR is available, the $\Sigma - D$ relation can be the only tool to estimate the distance to such objects. The empirical $\Sigma - D$ relation was examined in numerous works (Case and Bhattacharya 1998, Berkhuijsen 1986, Arbutina and Urošević 2005, Urošević et al. 2010, Pavlović et al. 2013, Pavlovic et al. 2014, Vukotić et al. 2019). The $\Sigma-D$ relations are derived from the "calibrating sample" (calibrators) of the shell SNRs detected at radio-wavelengths, with independently obtained distances of acceptable accuracy.

Here we present an updated sample of calibrators for the Galactic $\Sigma-D$ relation, with the most reliable independent distance estimates available in the literature (Section 2). The method used for calibration is described in Section 3. Calibrations and estimated $\Sigma - D$ distances to Galactic SNRs without reliable distance estimates are presented in Section 4 and a summary of the work is given in the last Section.

2. CALIBRATORS SELECTION AND DISTANCE UPDATES

In Table 1, we present the calibrating sample consisting of 69 SNRs with reliable distance estimates. For calibration of the $\Sigma - D$ relation, we choose SNRs whose radio-emission is non-thermal, and whose structure in the radio-domain is shell-like. The starting point in our search for calibrators were catalogs by Green (2025) and Ferrand and Safi-Harb (2012)[1], as well as the paper by Ranasinghe and Leahy (2022), where they listed 215 SNRs (and SNR candidates) in our Galaxy, with derived distances. The recent studies by Zhou et al. (2023) and Chen et al. (2025) have derived or improved distances to over 150 SNRs and 170 SNR candidates. Distances to SNRs in our calibrating sample were determined from coincidences with the observed H II regions and molecular clouds, or association with the red clump stars, pulsars, H I absorption features and polarization, Hα line radial velocity, or optical proper motion measurements. Many of distance estimates are taken from the works of Ranasinghe and Leahy (2022) and Ranasinghe and Leahy (2018b), who, for consistency, recalculated kinematic distances from literature using the values presented by Reid et al. (2014). Chen et al. (2025) presented the extinction–distance method that combines precise Gaia DR3 photometry, parallax, and stellar parameters from the SHBoost catalog (Khalatyan et al. 2024) to construct extinction–distance profiles for 44 Galactic SNRs associated with a neutron star. Zhou et al. (2023) derived kinematic distances to SNRs that are associated with molecular clouds in the coverage of the Milky Way Imaging Scroll Painting (MWISP[2]) project. The list of all distance references is given below Table 1.

This paper is the fourth in a row of papers studying the empirical $\Sigma - D$ relation by the Belgrade SNR group: Paper I - Pavlović et al. (2013); Paper II - Pavlovic et al. (2014); Paper III - Vukotić et al. (2019). In Paper I, the sample had 60 SNRs (55 shell-like and 5 composite), and in Paper II, 65 calibrators (60 shell-like and 5 composite with a pure shell structure in the radio domain). These five composite SNRs are: G11.2-0.3, G93.3+6.9 (DA 530), G189.1+3.0 (IC 443), G338.3-0.0, and G344.7-0.1. Paper III had almost twice as many calibrators - 110. As discussed in Vukotić et al. (2019), the list of 110 calibrators had 19 SNRs marked as objects with poor distance estimates, as well as 33 mixed-morphology SNRs. As noted in Paper III, the mixed-morphology SNRs do not follow a classical SNR evolution and so can hardly be represented by the Sedov-Taylor model, which is assumed in derivation of theoretical $\Sigma-D$ relation. Therefore, we did not use mixed-morphology SNRs as calibrators in this work. Additionally, the youngest Galactic SNR G1.9+0.3 which is in the flux density increasing phase of free expansion (as shown in Pavlović (2017) and references therein) is also excluded from the set of calibrators (as done in Papers I, II and III). Here, we also excluded the SNRs whose distance estimates might be taken as unreliable. In the cases when independent estimates did not match within the error bars, or if the error bars were too large, we would consider such distance estimate unreliable. In cases where multiple distances to a single SNR could be considered as reliable estimates, the average value of these distances was calculated and subsequently used to calibrate the Galactic $\Sigma - D$ relation. Distance estimates and references used for 69 calibrating SNR in this paper are presented in Table 1. Radio fluxes and size estimates were mainly taken from Green (2025). For SNRs whose type presented in the catalog by Green (2025) was designated with a question mark, we would visually check morphology in the radio-domain, and then decide whether we would consider that object as a shell (or partial-shell) or not. For partial shell SNRs the surface brightness was calculated as the measured radio flux spread over the surface as if the whole shell was observed. For this reason, in the list of calibrators, we include only partial shells with more than 70% of the shell visible in radio-image. Also, we did not use as calibrators the SNRs whose geometry is highly elongated, since their surrounding ISM is probably very non-uniform, and their evolution rather complex. At the end, instead of five composite SNRs used in Papers I, II, and III, we use G11.2-0.3 and DA 530 as calibrators because of their clear separation between the shell and central field radio emission.

After applying these filters on SNRs listed in the catalog in Green (2025) - shell (or partial-shell) mor-

[1] http://snrcat.physics.umanitoba.ca/

[2] http://www.radioast.nsdc.cn/mwisp.php

Table 1: Calibration sample for $\Sigma - D$ relation, consisting of 69 shell SNRs, with known distances.

No.	name	other names	$S_{1\mathrm{GHz}}$ [Jy]	θ_1 [arcmin]	θ_2 [arcmin]	distance [kpc]	D [pc]	$\log\Sigma$ [$\mathrm{Wm^{-2}Hz^{-1}sr^{-1}}$]	References[1]
1	G4.5+6.8	Kepler, SN1604	19.0	3.0	3.0	5.1	4.5	-18.50	1
2	G8.7-0.1	W30	80.0	45.0	45.0	3.7	48.4	-20.23	4, 3, 66
3	G9.7-0.0		3.7	15.0	11.0	4.3	16.1	-20.47	4, 3, 66
4	G11.0-0.0		1.3	11.0	9.0	2.7	7.8	-20.70	5, 66
5	G11.2-0.3*		22.0	4.0	4.0	3.3	3.8	-18.68	3, 66
6	G12.8-0.0	W33	0.8	3.0	4.0	4.3	4.3	-20.00	6, 66
7	G15.4+0.1		5.6	15.0	14.0	3.0	12.6	-20.40	66
8	G18.1-0.1*		4.6	8.0	8.0	6.0	14.0	-19.97	9, 8, 66
9	G18.6-0.2		1.4	6.0	8.0	4.2	8.5	-20.36	9, 66
10	G18.8+0.3	Kes 67	33.0	17.0	11.0	13.6	54.1	-19.58	9, 66
11	G21.8-0.6*	Kes 69	65.0	20.0	20.0	4.7	27.3	-19.61	10, 9, 8, 66
12	G22.7-0.2		33.0	26.0	26.0	4.6	34.8	-20.13	11, 9, 66
13	G23.3-0.3	W41	70.0	27.0	27.0	4.8	37.7	-19.84	9, 66
14	G28.6-0.1		5.4	10.8	10.8	8.9	28.0	-20.16	12, 66
15	G29.6+0.1		0.6	5.0	5.0	4.7	6.8	-20.46	13, 66
16	G31.9+0.0	3C391	25.0	7.0	5.0	7.2	12.4	-18.97	14, 66
17	G32.4+0.1	Kes 32	0.8	6.0	6.0	10.7	18.7	-20.47	3, 66
18	G32.8-0.1	Kes 78	12.0	17.0	10.0	5.0	19.0	-19.97	9, 66
19	G33.6+0.1	Kes 79, HC13	13.5	10.0	10.0	4.3	12.5	-19.69	9, 66
20	G35.6-0.4		9.0	10.0	8.0	3.4	8.8	-19.77	9, 66
21	G43.3-0.2	W49B	38.0	4.0	3.0	9.5	9.6	-18.32	9, 66
22	G54.4-0.3	HC40	28.0	40.0	40.0	5.9	68.6	-20.58	14, 66
23	G55.0+0.3*		0.6	20.0	15.0	4.3	21.7	-21.54	66
24	G74.0-8.5	Cygnus Loop	210.0	200.0	170.0	0.7	38.9	-21.03	17
25	G78.2+2.1	DR4, gamma Cygni SNR	320.0	60.0	60.0	1.8	31.4	-19.87	5, 3, 66, 67
26	G82.2+5.3*	W63	120.0	95.0	65.0	3.2	73.1	-20.53	5, 18, 66
27	G84.2-0.8*		11.0	20.0	16.0	7.0	36.4	-20.29	19 , 3
28	G89.0+4.7	HB21	220.0	120.0	90.0	1.9	57.4	-20.51	5, 18, 66, 67
29	G93.7-0.2*	CTB 104A, DA 551	65.0	80.0	80.0	1.9	44.2	-20.82	21, 10, 18
30	G94.0+1.0*	3C434.1	13.0	30.0	25.0	2.5	19.9	-20.58	22, 18, 3, 66
31	G108.2-0.6		8.0	70.0	54.0	3.0	53.7	-21.50	24, 66
32	G109.1-1.0	CTB 109	20.0	28.0	28.0	3.1	25.2	-20.42	25, 66, 67
33	G111.7-2.1	Cassiopeia A	2300.0	5.0	5.0	3.3	4.8	-16.86	26, 66, 69
34	G114.3+0.3*		5.5	90.0	55.0	0.7	14.3	-21.78	27, 3, 67
35	G116.5+1.1*		10.0	80.0	60.0	1.3	26.2	-21.50	27, 3
36	G116.9+0.2*	CTB 1	8.0	34.0	34.0	2.7	26.7	-20.98	27, 3, 66
37	G120.1+1.4*	Tycho, SN1572	50.0	8.0	8.0	3.3	7.7	-18.93	29, 66, 69
38	G127.1+0.5	R5	12.0	45.0	45.0	0.6	7.9	-21.05	30, 66
39	G132.7+1.3	HB3	45.0	80.0	60.0	1.9	38.3	-20.85	31, 66, 67
40	G152.4-2.1		3.5	100.0	95.0	1.5	42.5	-22.26	32, 66
41	G156.2+5.7		5.0	110.0	110.0	1.7	54.4	-22.21	33
42	G160.9+2.6	HB9	110.0	140.0	120.0	0.8	30.2	-21.01	34, 67
43	G180.0-1.7	S147	65.0	180.0	180.0	1.3	68.1	-21.52	35, 66, 67, 68
44	G190.9-2.2		1.3	70.0	60.0	1.3	24.5	-22.33	36, 66
45	G205.5+0.5*	Monoceros Nebula	140.0	220.0	220.0	1.7	108.8	-21.36	36, 66
46	G206.9+2.3*	PKS 0646+06	6.0	60.0	40.0	2.3	32.8	-21.42	37, 66
47	G213.0-0.6		21.0	160.0	140.0	1.2	52.2	-21.85	36
48	G260.4-3.4*	Puppis A, MSH 08-44	130.0	60.0	50.0	1.5	23.9	-20.19	38, 3, 67
49	G290.1-0.8	MSH 11-61A	42.0	19.0	14.0	4.8	22.8	-19.62	41, 3, 67
50	G292.2-0.5		7.0	20.0	15.0	8.1	40.8	-20.45	42, 3
51	G296.8-0.3	1156-62	9.0	20.0	14.0	9.3	45.3	-20.32	44, 3
52	G306.3-0.9		0.2	4.0	4.0	20.0	23.3	-20.82	45
53	G309.2-0.6		7.0	15.0	12.0	2.8	10.9	-20.23	40
54	G311.5-0.3*		3.7	4.0	4.0	12.6	14.7	-19.46	46, 3

...Table 1. continued

No.	name	other name	$S_{1\mathrm{GHz}}$ [Jy]	θ_1 [arcmin]	θ_2 [arcmin]	distance [kpc]	D [pc]	$\log\Sigma$ [$\mathrm{Wm^{-2}Hz^{-1}sr^{-1}}$]	References
55	G315.4-2.3	RCW 86, MSH 14-63	49.0	42.0	42.0	2.2	26.9	-20.38	40, 3
56	G327.4+0.4	Kes 27	25.3	21.0	21.0	4.3	26.3	-20.06	47, 3
57	G327.6+14.6	SN1006	19.0	30.0	30.0	2.0	17.5	-20.50	48, 49
58	G332.4-0.4	RCW 103	28.0	100.0	100.0	2.8	81.4	-21.38	40, 67
59	G332.4+0.1	MSH 16-51, Kes 32	26.0	15.0	15.0	7.5	32.7	-19.76	50, 3
60	G337.0-0.1	CTB 33	1.5	1.5	1.5	11.0	4.8	-19.00	52, 53
61	G337.2-0.7		1.5	6.0	6.0	9.0	15.7	-20.20	54, 3
62	G337.8-0.1	Kes 41	15.0	9.0	6.0	12.3	26.3	-19.38	55, 3
63	G340.6+0.3		5.0	6.0	6.0	15.0	26.2	-19.68	56
64	G343.1-0.7**		7.8	27.0	21.0	4.9	33.9	-20.68	3
65	G346.6-0.2*		8.0	8.0	8.0	10.4	24.2	-19.73	57, 3
66	G348.7+0.3	CTB 37B	26.0	12.0	12.0	13.2	46.1	-19.57	58
67	G352.7-0.1		4.0	8.0	6.0	7.5	15.1	-19.90	61
68	G353.6-0.7		2.5	30.0	30.0	3.0	26.2	-21.38	62, 63
69	G359.1-0.5*		14.0	24.0	24.0	2.7	18.8	-20.44	64, 65, 67

References: (1) Sankrit et al. (2016); (2) Velázquez et al. (2002); (3) Ranasinghe and Leahy (2022); (4) Hewitt and Yusef-Zadeh (2009); (5) Shan et al. (2018); (6) Halpern et al. (2012); (7) Su et al. (2017); (8) Lee et al. (2020); (9) Ranasinghe and Leahy (2018b); (10) Wang et al. (2020); (11) Sofue et al. (2021); (12) Ranasinghe and Leahy (2018a); (13) Ranasinghe et al. (2018); (14) Ranasinghe and Leahy (2017); (15) Supan et al. (2018); (16) Zhou et al. (2020); (17) Fesen et al. (2021); (18) Zhao et al. (2020); (19) Leahy and Green (2012); (20) Booth et al. (2022); (21) Uyaniker et al. (2002); (22) Jeong et al. (2013); (23) Kothes et al. (2005); (24) Tian et al. (2007b); (25) Sánchez-Cruces et al. (2018); (26) Alarie et al. (2014); (27) Yar-Uyaniker et al. (2004); (28) Pineault et al. (1993); (29) Hayato et al. (2010); (30) Leahy and Tian (2006); (31) Zhou et al. (2016); (32) Foster et al. (2013); (33) Katsuda et al. (2016); (34) Leahy and Tian (2007); (35) Dinçel et al. (2015); (36) Yu et al. (2019); (37) Ambrocio-Cruz et al. (2014); (38) Reynoso et al. (2017); (39) Allen et al. (2015); (40) Shan et al. (2019); (41) Reynoso et al. (2006); (42) Caswell et al. (2004); (43) Giacani et al. (2000); (44) Gaensler et al. (1998); (45) Sawada et al. (2019); (46) Andersen et al. (2011); (47) McClure-Griffiths et al. (2001); (48) Raymond et al. (2017); (49) Winkler et al. (2003); (50) Vink (2004); (51) Zhu et al. (2015); (52) Frail et al. (1996); (53) Combi et al. (2005); (54) Takata et al. (2016); (55) Koralesky et al. (1998); (56) Kothes and Dougherty (2007); (57) Sano et al. (2021); (58) Tian and Leahy (2012); (59) Tian and Leahy (2014); (60) Tian et al. (2007a); (61) Giacani et al. (2009); (62) Tian et al. (2010); (63) Doroshenko et al. (2023); (64) Ogbodo et al. (2020); (65) Eppens et al. (2020); (66) Zhou et al. (2023); (67) Chen et al. (2025).

phology in radio domain; available radio-flux at 1 GHz (or estimates at other frequencies, but with known spectral index); reliable distance - our sample has 69 Galactic SNRs, which were used to derive the empirical $\Sigma - D$ relation.

3. METHOD DESCRIPTION

A two-parameter straight line, fitted to the sample of calibrators is used for distance (d) estimates:

$$\log\Sigma = \log A + \beta \log D, \qquad (2)$$

where $\log A$ and β are fit parameters in the $\log\Sigma - \log D$ space. The fit is usually performed with vertical offsets, on the $\log\Sigma$ axis. This fit type does not give stable results and is not consistent when using offsets on the $\log D$ axis in a sense that it gives a different calibration for distance determination when compared to the case that uses $\log\Sigma$ offsets. The fits with orthogonal offsets give stable and consistent results and should be used for distance calibration (Urošević et al. 2010, Pavlović et al. 2013).

While fitting a line through the data points is a practical way to describe the calibration, this approach reduces all the information contained in the calibrating sample to just two parameters that define the best-fit line. Given that the evolution of SNRs spans over multiple orders of magnitude in surface brightness Σ (to a lesser part also in D) and that SNRs expand in interstellar matter (ISM) environments of different density and consistency, the $\Sigma - D$ relation exhibits a large scatter. Some areas of the $\Sigma - D$ plane may have data points that are systematically positioned away from the best fit line. Instead of a two-parameter fit line, it is more consistent to use a matrix that describes the data points density in the $\Sigma - D$ plane. This gives a more consistent calibration and includes more information from the calibrating sample if compared to just using a two-parameter fit line.

The uncertainties of orthogonal fit parameters were calculated as standard deviation from the mean values of bootstrap resamples with repetition using a random number generator (Saito and Matsumoto 2008). The matrix of probability density function for data distribution in the $\Sigma - D$ plane was calculated using Gaussian kernel. The kernel widths in both dimensions were calculated from maximum likelihood

”leave one out” cross validation (Duin 1976). We have updated the code from paper III (Vukotić et al. 2019) for calculation of median value. In the previous version of the code, the values for mode and median were off by a few percent on average due to the code error, which is now corrected. For each resolved value of $\log \Sigma$, from the matrix of probability density function, a median value along the $\log D$ axis was used for distance calibration in order to calculate distances to objects with literature values of flux density at 1GHz ($S_{\rm 1GHz}$) and angular diameters (θ_1 and θ_2). The corresponding 1GHz radio surface brightness was calculated as:

$$\Sigma_{\rm 1GHz} = \frac{S_{\rm 1GHz}}{\Omega} = \frac{S_{\rm 1GHz}}{\pi \theta_1 \theta_2}, \tag{3}$$

where Ω is the solid angle of SNR, while angular diameters θ_1 and θ_2 are related to distance as $\theta_1 = 2a/d$, $\theta_2 = 2b/d$, a and b being major and minor semi-axes of SNR. In this notation, we calculate the diameter of SNR as $D = \sqrt{\theta_1 \theta_2}$.

For presented calibrations, we calculate the distance fractional error for the entire calibrating sample as:

$$f = \frac{100\%}{n} \times \sum_{i=1}^{n} \frac{|d_i - d_{\rm c}|}{d_i}, \tag{4}$$

where d_i is the i-th SNR distance, $d_{\rm c}$ is the distance calculated from the calibration, while n is the number of calibrators.

4. ANALYSIS OF RESULTS: $\Sigma - D$ DISTANCES TO GALACTIC SNRs

In Fig. 1, we present the calibrating sample and corresponding $\Sigma - D$ calibration for distance determination. The distance fractional errors are large, with similar values obtained from both methods: the orthogonal offsets fit, and the kernel smoothing (calculated median value) - see Fig. 1. The values of the fit parameter uncertainties are indicative of the large data scatter.

Even with the most reliable distances for calibrators it is evident that $\Sigma - D$ relation has a significant intrinsic scatter, which can partly be caused by distance determination uncertainties, but also with the diversity of the SNR environments and their parameters.

A dozen of young and bright remnants are the cause of a statistically significant elongation from the rest of the sample. The majority of the sample is elliptically shaped and well grouped in the (10−100) pc diameter range and (−19, −22) in the $\log \Sigma$ range. This part of the sample shows a steeper $\log \Sigma - \log D$ slope, than the value of −5 from the orthogonal fit-line. Such a steeper slope is in marginal agreement with slopes from theoretical models (which are between -6 and -4) for SNRs expanding in a uniform density ISM (Pavlović et al. 2018), and is likely to be indicative of SNRs reaching the environments of the

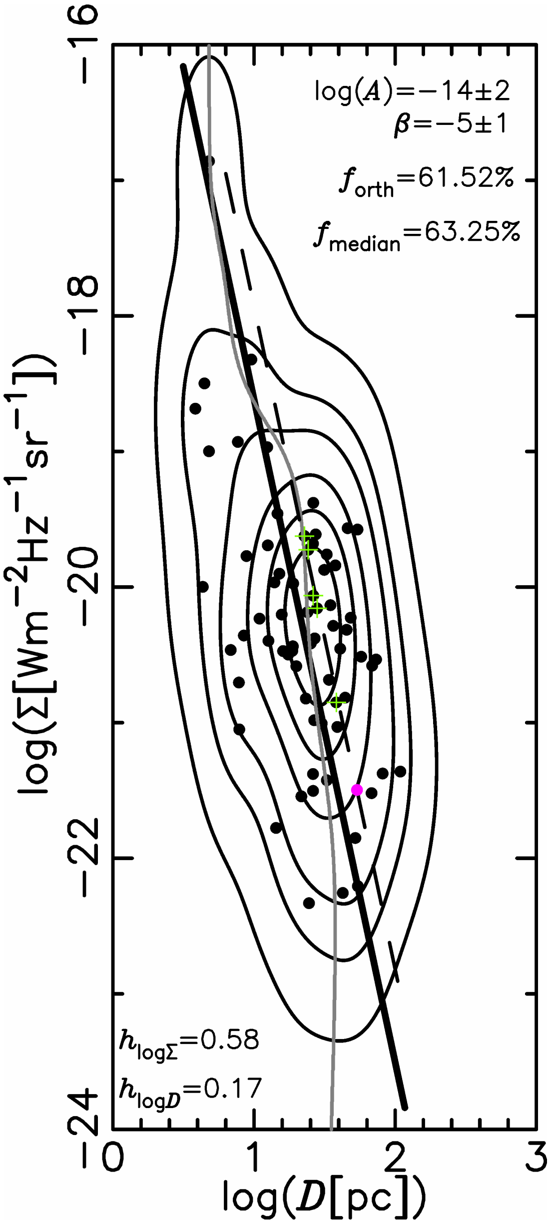

Fig. 1: Calibration SNR sample consisting of 86 calibrators with reliable distances. The black thick line presents the orthogonal offsets fit while the thin gray line designates median values of diameter distributions for the corresponding surface brightness values for the data normalized probability density matrix (contours). Contour levels are at 0.01, 0.05, 0.1, 0.2, 0.3, 0.4, and 0.5. The orthogonal fit parameters, optimal kernel widths h for data probability density calculation, and fractional distance errors f for both, orthogonal fit, and median values of diameter distributions at corresponding surface brightness values are designated in the plot. Cygnus Loop SNR is designated with a purple dot. Thin dashed line is the orthogonal fit translated along the horizontal axis to the position of Cygnus Loop. Calibrators that are within 0.02 on the $\log D$ axis from the dashed line are additionally designated with green crosses.

increased ISM density during their evolution (Kostić et al. 2024). Moreover, an inspection of Fig. 1 clearly shows steeper slopes in some segments of the pdf line in comparison to the orthogonal fit-line. This can be interpreted by particular evolution and selection effects. The bump near surface brightness 10^{-19} W/(m^{2}Hz sr) can probably be explained by the evolution effect of transition from the free expansion to the Sedov evolution phase. Biases in this range of the high radio surface brightnesses should not be active. On the other hand, for the obvious steeper slope of the pdf line in the range of the surface brightness near and below 10^{-22} W/(m^{2}Hz sr), the Malmquist bias should be responsible for the steepening due to missing of the large diameter and low surface brightness SNRs from the sample (obvious missing of objects in the lower-right part of the $\Sigma - D$ plane, right to the orthogonal fit near and below 10^{-22} W/(m^{2}Hz sr)). We emphasize here that the Malmquist bias also has influence on appearing of the steeper slope of the orthogonal fit-line in Fig. 1. but to a lesser extent than to the pdf calibration (see also the last column of Tables 2 and 3 where difference between the orthogonal fit and pdf derived distances is positive for the dimmer objects). For this reason, the orthogonal fit distances should only be used for dimmer objects with the 1 GHz brightness $\lesssim 10^{-22}$ W/(m^{2}Hz sr). For brighter objects, the pdf method gives more realistic distances compared to the distances calculated from the orthogonal fit parameters.

This likely contributes to a large scatter of the data in the $\Sigma - D$ plane, even when the distances are reliable, and such samples are not to be described by a single straight line fit, in which case, the estimated distances should be less accurate than when the data density based calibration methods are used.

Cygnus Loop is a shell-like SNR with the most reliable distance estimate: 725±15 pc (Fesen et al. 2021). Its distance is determined by using parallaxes from the *Gaia* mission for stars being in front, and just behind of the shock front. Due to this, in Fig. 1, an orthogonal fit-line (thin dashed black line) is drown through the Cygnus Loop (purple dot), as probably the best calibrator in the entire calibration sample. This line allows us to visually check the difference between the orthogonal fit through the full sample, and the line shifted according to one SNR with probably the best derived distance. Additionally, calibrators that are within 0.02 on the $\log D$ axis from the dashed line are designated with the green crosses in Fig. 1. These objects represent calibrators that probably share approximately the same evolutionary track with Cygnus Loop, and should be evolutionary younger "cousins" of the Cygnus Loop.

In Table 2 we present distances to 164 Galactic shell and partial-shell SNRs (cataloged in Green 2025) that do not have reliable distance estimates in literature. Distances to these SNRs were calculated using the calibrations from Fig. 1. We also searched literature for recently discovered objects designated as SNRs or SNR candidates with shell-like morphology, not present in the catalog given by Green (2025). We found 27 of these objects and they are listed in Table 3. We give their names, the surface brightness at 1 GHz, angular size, spectral index and calculated distance, and physical diameter. Majority of these new SNR candidates are discovered with: The H I/OH/Recombination line survey of the Milky Way – THOR Beuther et al. (2016); D-configuration Very Large Array (VLA-D) continuum images of the 4–8 GHz global view on star formation (GLOSTAR) survey; LOFAR (LOw Frequency ARray) Two-Metre Sky Survey.

When using distances obtained by the $\Sigma - D$ method, one should especially be careful with the interpretation in cases of partial shells or elogated SNRs, or SNRs without derived spectral index, etc. In such cases, the $\Sigma - D$ distance should be used as indication of probable distance.

5. SUMMARY

We did a literature search for updates on reliable distances for Galactic SNRs. The calibration of the $\Sigma - D$ relation was calculated using fitting of the straight line to the $\Sigma - D$ data of 69 calibrators with reliable distance estimates, but also with using the median values of the diameter distribution for each fixed value of Σ, from the calculated probability density of data points in the $\Sigma - D$ plane. The later method has a higher fidelity in showcasing the calibrating sample, when compared to the fitting method, likely because of the discrepancy caused by the SNRs that continued their expansion into more dense regions of the ISM (Kostić et al. 2024). This is reflected in the contour lines (Fig. 1) giving an impression of steeper $\Sigma - D$ slopes (on some large segments in the $\Sigma - D$ diagram) than the orthogonal fit line. These steeper slopes are in marginal agreement with the simulated $\Sigma - D$ slopes (between -4 and -6) obtained for SNRs expanding in ISM of uniform density (Pavlović et al. 2018).

Due to such a slope discrepancy, methods based on data density in the $\Sigma - D$ plane should be preferred to fitting methods when calibrating the $\Sigma - D$ relation for the purpose of distance estimates, except for the very low surface brightness objects with 1 GHz brightness $\lesssim 10^{-22}$ W/(m^{2}Hz sr).

With the calibrations presented in Fig. 1 and Table 1, we have calculated distances to 164 Galactic SNRs that do not have previously determined reliable distance estimates (Table 2). Also, in Table 3, we give distances to 27 recently discovered SNR candidates by new radio facilities, such as Australian Square Kilometer Array Pathfinder (ASKAP), Expanded Very Large Array (EVLA), The Murchison Widefield Array (MWA), and LOFAR radio interferometers.

Table 2: Data and calculated $\Sigma - D$ distances for 164 shell SNRs that do not have reliable distances determined by other methods. $S_{1\mathrm{GHz}}$ is flux density at 1 GHz, θ_1 and θ_2 are angular major and minor axe of SNR, Σ is surface brightness at 1 GHz, d_{orth} and D_{ort} are distance and physical diameter obtained from orthogonal fit calibration, while d_{median} and D_{median} are obtained from data probability density calculation.

N	name	$S_{1\mathrm{GHz}}$ [Jy]	θ_1 x θ_2 [arcmin]	$\log(\Sigma)$ $\Sigma[\frac{\mathrm{W}}{\mathrm{m^2\,Hz\,sr}}]$	α	d_{orth} [kpc]	D_{ort} [pc]	d_{median} [kpc]	D_{median} [pc]	Δd [kpc]
1	G0.3+0.0	22.0	15x8	-19.56	0.60	4.9	16	6.9	22	-2.0
2	G1.0-0.1	15.0	8x8	-19.45	0.60	6.4	15	9.2	21	-2.8
3	G1.4-0.1*	2.0	10x10	-20.52	0.55	8.4	25	8.7	25	-0.2
4	G3.1-0.6	5.0	52x28	-21.29	0.90	3.2	35	2.8	31	0.4
5	G3.7-0.2	2.3	14x11	-20.65	0.65	7.2	26	7.2	26	0.0
6	G3.8+0.3	3.0	18x18	-20.86	0.60	5.5	29	5.2	27	0.3
7	G4.2-3.5	3.2	28x28	-21.21	0.60	4.2	34	3.7	30	0.4
8	G4.8+6.2	3.0	18x18	-20.86	0.60	5.5	29	5.2	27	0.3
9	G5.2-2.6	2.6	18x18	-20.92	0.60	5.6	30	5.3	28	0.3
10	G5.5+0.3	5.5	15x12	-20.34	0.70	5.8	22	6.2	24	-0.5
11	G5.9+3.1	3.3	20x20	-20.91	0.40	5.1	29	4.7	28	0.3
12	G6.1+0.5	4.5	18x12	-20.50	0.90	5.7	24	5.8	25	-0.2
13	G6.4-0.1*,**	48.0	310x48	-21.31	0.55	1.0	36	0.9	31	0.1
14	G6.4+4.0	1.3	31x31	-21.69	0.40	4.7	43	3.8	35	0.9
15	G6.5-0.4	27.0	18x18	-19.90	0.60	3.5	18	4.4	23	-0.9
16	G7.0-0.1	2.5	15x15	-20.78	0.50	6.3	28	6.1	27	0.2
17	G7.2+0.2	2.8	12x12	-20.53	0.60	7.1	25	7.2	25	-0.1
18	G7.7-3.7	11.0	22x22	-20.47	0.32	3.7	24	3.9	25	-0.1
19	G8.3+0.0	1.2	5x4	-20.04	0.65	15.1	20	18.1	23	-3.0
20	G8.7-5.0	44.0	26x26	-20.01	0.30	2.5	19	3.1	23	-0.5
21	G8.9+0.4	9.0	24x24	-20.63	0.60	3.7	26	3.7	26	0.0
22	G9.8+0.6	3.9	12x12	-20.39	0.50	6.6	23	7.0	24	-0.4
23	G9.9-0.8	6.7	12x12	-20.15	0.40	5.9	21	6.8	24	-0.9
24	G11.1-0.7	1.0	11x7	-20.71	0.70	10.5	27	10.3	26	0.2
25	G11.1+0.1	2.3	12x10	-20.54	0.40	7.8	25	7.9	25	-0.1
26	G11.4-0.1	6.0	8x8	-19.85	0.50	7.7	18	9.9	23	-2.2
27	G11.8-0.2	0.7	4x4	-20.18	0.30	18.0	21	20.5	24	-2.5
28	G12.2+0.3	0.8	6x5	-20.40	0.70	14.5	23	15.5	25	-1.0
29	G12.7-0.0	0.8	6x6	-20.48	0.80	13.8	24	14.3	25	-0.6
30	G13.1-0.5	11.0	38x28	-20.81	0.60	3.0	28	2.8	27	0.1
31	G13.5+0.2	3.5	5x4	-19.58	1.00	12.1	16	16.9	22	-4.8
32	G14.1-0.1	0.5	6x5	-20.60	0.60	16.0	25	16.0	26	-0.0
33	G15.1-1.6	5.5	30x24	-20.94	0.00	3.8	30	3.6	28	0.2
34	G15.9+0.2	5.0	7x5	-19.67	0.63	9.5	16	13.0	22	-3.5
35	G16.0-0.5**	10.0	2.7x15	-19.43	0.60	7.9	15	11.4	21	-3.5
36	G16.2-2.7	2.5	17x17	-20.89	0.40	5.9	29	5.5	27	0.4
37	G17.0-0.0	0.5	5x5	-20.52	0.50	16.9	25	17.3	25	-0.4
38	G17.4-0.1	0.4	6x6	-20.78	0.70	15.8	28	15.2	27	0.6
39	G17.4-2.3	5.0	24x24	-20.88	0.50	4.2	29	3.9	27	0.2
40	G17.8-2.6	5.0	24x24	-20.88	0.50	4.2	29	3.9	27	0.2
41	G17.8+16.7	2.7	51x45	-21.75	0.80	3.1	44	2.5	35	0.6
42	G19.1+0.2	10.0	27x27	-20.69	0.50	3.4	26	3.3	26	0.1
43	G21.0-0.4	1.1	9x7	-20.58	0.60	10.9	25	11.1	26	-0.1
44	G21.6-0.8	1.4	13x13	-20.90	0.50	7.8	29	7.3	28	0.5
45	G21.8-3.0	5.0	60x60	-21.68	0.70	2.4	42	2.0	34	0.5
46	G24.7-0.6**	15.0	8x30	-20.03	0.50	4.3	19	5.2	23	-0.9
47	G25.1-2.3	8.0	80x30	-21.30	0.50	2.5	35	2.2	31	0.3
48	G27.4+0.0	6.0	4x4	-19.25	0.68	11.6	13	16.9	20	-5.3
49	G28.3+0.2	1.3	10x10	-20.71	0.70	9.2	27	9.0	26	0.2
50	G28.7-0.4	0.9	9x9	-20.78	0.80	10.6	28	10.2	27	0.4

Continued on next page...

...Table 2. continued

N	name	$S_{1\mathrm{GHz}}$ [Jy]	θ_1xθ_2 [arcmin]	log(Σ) $\Sigma[\frac{\mathrm{W}}{\mathrm{m^2\,Hz\,sr}}]$	α	d_{orth} [kpc]	D_{ort} [pc]	d_{median} [kpc]	D_{median} [pc]	Δd [kpc]
51	G31.5-0.6*	2.0	18x18	-21.03	0.55	6.0	31	5.5	29	0.5
52	G32.0-4.9	22.0	60x60	-21.04	0.50	1.8	31	1.6	29	0.1
53	G34.7-0.4	27.0	240x35	-21.32	0.37	1.3	36	1.2	31	0.2
54	G36.6-0.7	1.0	25x25	-21.62	0.70	5.7	41	4.7	34	1.0
55	G36.6+2.6	0.7	17x13	-21.32	0.50	8.3	36	7.3	31	1.0
56	G40.5-0.5	11.0	22x22	-20.47	0.40	3.7	24	3.9	25	-0.1
57	G41.1-0.3	2.5	25x4.5	-20.48	0.50	7.8	24	8.1	25	-0.3
58	G41.5+0.4*	1.0	10x10	-20.82	0.55	9.7	28	9.3	27	0.4
59	G42.0-0.1*	0.5	8x8	-20.93	0.55	12.8	30	11.9	28	0.9
60	G42.8+0.6	3.0	24x24	-21.11	0.50	4.6	32	4.2	29	0.4
61	G43.9+1.6	9.0	60x60	-21.42	0.50	2.1	38	1.8	32	0.3
62	G45.7-0.4	4.2	22x22	-20.88	0.40	4.5	29	4.3	27	0.3
63	G46.8-0.3	16.0	15x15	-19.97	0.54	4.3	19	5.3	23	-1.0
64	G49.2-0.7	160.0	30x30	-19.57	0.30	1.8	16	2.5	22	-0.7
65	G51.04+0.07**	3.0	1.8x7.5	-19.48	0.55	14.0	15	20.1	21	-6.1
66	G53.4+0.0	1.5	10x10	-20.65	0.60	8.9	26	8.9	26	0.0
67	G53.6-2.2	8.0	33x28	-20.89	0.50	3.3	29	3.1	27	0.2
68	G55.7+3.4	1.0	23x23	-21.55	0.30	5.9	40	5.0	33	0.9
69	G57.2+0.8**	12.0	1.8x12	-19.08	0.35	9.2	12	12.7	17	-3.5
70	G59.5+0.1*	3.0	15x15	-20.70	0.55	6.1	27	6.0	26	0.1
71	G64.5+0.9	0.15	8x8	-21.45	0.50	16.3	38	14.0	33	2.4
72	G65.1+0.6	5.5	90x50	-21.74	0.61	2.2	43	1.8	35	0.4
73	G65.3+5.7	42.0	310x340	-22.22	0.60	0.6	55	0.4	37	0.2
74	G67.7+1.8	1.0	15x12	-21.08	0.61	8.2	32	7.5	29	0.7
75	G69.7+1.0	2.0	16x14	-20.87	0.70	6.6	29	6.3	27	0.4
76	G73.9+0.9	9.0	27x27	-20.73	0.23	3.4	27	3.4	26	0.1
77	G83.0-0.3	1.0	9x7	-20.62	0.40	11.1	26	11.1	26	0.0
78	G93.3+6.9*,**	20.0	9x27	-19.91	0.45	4.0	18	5.1	23	-1.1
79	G96.0+2.0*,**	26.0	0.3x26	-18.37	0.60	10.1	9	8.9	8	1.3
80	G114.3+0.3	5.5	90x55	-21.78	0.50	2.2	44	1.7	35	0.4
81	G119.5+10.2**	90.0	36x90	-20.38	0.60	1.4	23	1.5	24	-0.1
82	G126.2+1.6	6.0	70x70	-21.73	0.50	2.1	43	1.7	35	0.4
83	G166.0+4.3	7.0	55x35	-21.26	0.37	2.7	35	2.4	31	0.3
84	G178.2-4.2	2.0	72x62	-22.17	0.50	2.7	53	1.9	37	0.8
85	G179.0+2.6	7.0	70x70	-21.67	0.40	2.1	42	1.7	34	0.4
86	G181.1+9.5	0.4	74x74	-22.96	0.40	3.6	77	1.7	37	1.9
87	G182.4+4.3	0.5	50x50	-22.52	0.40	4.3	63	2.6	38	1.7
88	G249.5+24.5	27.0	260x260	-22.22	0.70	0.7	55	0.5	37	0.2
89	G261.9+5.5	10.0	40x30	-20.90	0.40	2.9	29	2.7	28	0.2
90	G266.2-1.2**	120.0	50x120	-20.52	0.30	1.1	25	1.1	25	-0.0
91	G272.3-3.2	0.4	15x15	-21.57	0.60	9.2	40	7.7	34	1.5
92	G279.0+1.1	65.0	30x95	-20.46	0.60	1.5	24	1.6	25	-0.1
93	G284.3-1.8	11.0	24x24	-20.54	0.30	3.5	25	3.6	25	-0.1
94	G288.8-6.3	11.0	108x96	-21.80	0.41	1.5	45	1.2	35	0.3
95	G289.7-0.3	6.2	18x14	-20.43	0.20	5.1	24	5.3	25	-0.3
96	G294.1-0.0*	2.0	40x40	-21.73	0.55	3.7	43	3.0	35	0.7
97	G296.1-0.5	8.0	37x25	-20.89	0.60	3.3	29	3.1	27	0.2
98	G296.5+10.0	65.0	48x90	-20.65	0.50	1.4	26	1.4	26	0.0
99	G296.7-0.9	3.0	15x8	-20.42	0.50	7.4	23	7.7	25	-0.4
100	G298.6-0.0	50.0	12x9	-19.16	0.30	4.3	13	6.1	18	-1.8
101	G299.2-2.9*	0.5	18x11	-21.42	0.55	9.1	37	7.9	32	1.3
102	G299.6-0.5*	1.0	13x13	-21.05	0.55	8.3	31	7.6	29	0.7
103	G301.4-1.0*	2.1	37x23	-21.43	0.55	4.4	38	3.8	32	0.6

Continued on next page...

...Table 2. continued

N	name	$S_{1\mathrm{GHz}}$ [Jy]	θ_1xθ_2 [arcmin]	log(Σ) $\Sigma[\frac{\mathrm{W}}{\mathrm{m^2\,Hz\,sr}}]$	α	d_{orth} [kpc]	D_{ort} [pc]	d_{median} [kpc]	D_{median} [pc]	Δd [kpc]
104	G302.3+0.7	5.0	17x17	-20.58	0.40	5.1	25	5.2	26	-0.1
105	G304.6+0.1	14.0	8x8	-19.48	0.50	6.5	15	9.2	21	-2.8
106	G308.1-0.7*	1.2	13x13	-20.97	0.55	8.0	30	7.4	28	0.6
107	G308.4-1.4*	0.5	12x6	-20.98	0.55	12.3	30	11.4	28	0.9
108	G309.8+0.0	17.0	25x19	-20.27	0.50	3.4	22	3.8	24	-0.4
109	G310.6-0.3*	5.0	8x8	-19.93	0.55	8.0	19	10.0	23	-2.0
110	G310.8-0.4*	6.0	12x12	-20.20	0.55	6.0	21	6.9	24	-0.8
111	G312.4-0.4	45.0	38x38	-20.33	0.36	2.0	22	2.2	24	-0.2
112	G312.5-3.0*	3.5	20x18	-20.83	0.55	5.1	28	4.9	27	0.3
113	G315.4-0.3	8.0	24x13	-20.41	0.40	4.5	23	4.8	25	-0.3
114	G315.9-0.0*	0.8	25x14	-21.46	0.55	7.0	38	6.0	33	1.0
115	G316.3+0.0	20.0	29x14	-20.13	0.40	3.5	20	4.0	24	-0.6
116	G317.3-0.2*	4.7	11x11	-20.23	0.55	6.7	21	7.5	24	-0.8
117	G318.2+0.1*	3.9	40x35	-21.38	0.55	3.4	37	2.9	32	0.4
118	G321.9-0.3	13.0	31x23	-20.56	0.30	3.2	25	3.3	25	-0.0
119	G321.9-1.1*	3.4	28x28	-21.19	0.55	4.1	34	3.7	30	0.4
120	G323.5+0.1	3.0	13x13	-20.57	0.40	6.6	25	6.7	25	-0.1
121	G327.2-0.1*	0.5	5x5	-20.52	0.55	16.9	25	17.3	25	-0.4
122	G327.4+0.1*	1.9	14x14	-20.84	0.55	7.0	28	6.6	27	0.4
123	G329.7+0.4*	34.0	40x33	-20.41	0.55	2.2	23	2.3	25	-0.1
124	G330.0+15.0	350.0	180x180	-20.79	0.50	0.5	28	0.5	27	0.0
125	G330.2+1.0	5.0	11x11	-20.21	0.30	6.6	21	7.5	24	-0.9
126	G332.0+0.2	8.0	12x12	-20.08	0.50	5.7	20	6.7	23	-1.0
127	G332.5-5.6**	35.0	2x35	-19.12	0.70	5.2	13	7.4	18	-2.2
128	G332.4+0.1	26.0	15x15	-19.76	0.50	3.9	17	5.2	23	-1.3
129	G335.2+0.1	16.0	21x21	-20.26	0.50	3.6	22	4.0	24	-0.4
130	G336.7+0.5	6.0	14x10	-20.19	0.50	6.1	21	6.9	24	-0.8
131	G337.3+1.0	15.0	15x12	-19.90	0.55	4.7	18	5.9	23	-1.2
132	G338.1+0.4	4.0	15x15	-20.57	0.40	5.8	25	5.8	25	-0.1
133	G340.4+0.4	5.0	10x7	-19.97	0.40	7.8	19	9.6	23	-1.8
134	G341.9-0.3	2.5	7x7	-20.11	0.50	9.9	20	11.6	24	-1.7
135	G342.0-0.2	3.5	12x9	-20.31	0.40	7.3	22	8.0	24	-0.7
136	G342.1+0.9*	0.5	10x9	-21.08	0.55	11.5	32	10.5	29	1.0
137	G345.1-0.2	1.4	6x6	-20.23	0.70	12.3	21	13.7	24	-1.5
138	G345.1+0.2	0.6	10x10	-21.04	0.60	10.8	31	9.9	29	0.9
139	G345.7-0.2*	0.6	6x6	-20.60	0.55	14.6	25	14.6	26	-0.0
140	G347.3-0.5*	30.0	65x55	-20.90	0.55	1.7	29	1.6	28	0.1
141	G348.5-0.0**	10.0	10x10	-19.82	0.40	6.1	18	7.9	23	-1.8
142	G348.5+0.1	73.0	15x15	-19.31	0.30	3.2	14	4.6	20	-1.4
143	G348.8+1.1	0.6	10x10	-21.04	0.70	10.8	31	9.9	29	0.9
144	G349.2-0.1*	1.4	9x6	-20.41	0.55	10.9	23	11.5	25	-0.7
145	G349.7+0.2	2.0	20x2.5	-20.22	0.50	10.3	21	11.7	24	-1.3
146	G350.0-2.0	26.0	45x45	-20.71	0.40	2.1	27	2.0	26	0.0
147	G350.1-0.3	6.0	4x4	-19.25	0.80	11.6	13	16.9	20	-5.3
148	G351.7+0.8	14.0	10x18	-19.93	0.50	4.8	19	5.9	23	-1.2
149	G351.9-0.9*	1.8	12x9	-20.60	0.55	8.4	25	8.4	26	-0.0
150	G353.3-1.1	24.0	60x60	-21.00	0.85	1.8	31	1.6	28	0.1
151	G353.9-2.0	1.0	13x13	-21.05	0.50	8.3	31	7.6	29	0.7
152	G354.8-0.8*	2.8	19x19	-20.93	0.55	5.4	30	5.0	28	0.4
153	G355.4+0.7*	5.0	25x25	-20.92	0.55	4.1	30	3.8	28	0.3
154	G355.6-0.0*	3.0	8x6	-20.03	0.55	9.6	19	11.7	23	-2.0
155	G355.9-2.5	8.0	13x13	-20.15	0.50	5.4	21	6.3	24	-0.9
156	G356.2+4.5	4.0	25x25	-21.02	0.70	4.3	31	3.9	29	0.3

Continued on next page...

...Table 2. continued

N	name	$S_{1\mathrm{GHz}}$ [Jy]	θ_1xθ_2 [arcmin]	log(Σ) $\Sigma[\frac{\mathrm{W}}{\mathrm{m^2\,Hz\,sr}}]$	α	d_{orth} [kpc]	D_{ort} [pc]	d_{median} [kpc]	D_{median} [pc]	Δd [kpc]
157	G356.3-0.3*	3.0	11x7	-20.23	0.55	8.4	21	9.4	24	-1.0
158	G356.3-1.5*	3.0	20x15	-20.82	0.55	5.6	28	5.4	27	0.3
159	G357.7+0.3	10.0	24x24	-20.58	0.40	3.6	25	3.7	26	-0.0
160	G358.0+3.8*	1.5	38x38	-21.81	0.55	4.1	45	3.2	35	0.9
161	G358.1+1.0*	3.0	20x20	-20.95	0.55	5.2	30	4.8	28	0.4
162	G358.5-0.9*	4.0	17x17	-20.68	0.55	5.3	26	5.3	26	0.1
163	G359.0-0.9	23.0	23x23	-20.18	0.50	3.1	21	3.6	24	-0.4
164	G359.1+0.9*	2.0	12x11	-20.64	0.55	7.8	26	7.7	26	0.0

* SNRs without determined α and $S_{1\mathrm{GHz}}$. $S_{1\mathrm{GHz}}$ was calculated from available radio-flux and assuming $\alpha = -0.55$.

** Partial shell.

Table 3: Data and calculated $\Sigma - D$ distances for 27 recently discovered shell SNR candidates, not cataloged in Green (2025), that do not have distances determined by other methods. d_{orth} and D_{ort} are distance and physical diameter obtained from orthogonal fit calibration, while d_{median} and D_{median} are obtained from data probability density calculation. Δd is deference between d_{median} and d_{ort}.

N	name	$S_{1\mathrm{GHz}}$ [Jy]	θ_1xθ_2 [arcmin]	log(Σ) $\Sigma[\frac{\mathrm{W}}{\mathrm{m^2\,Hz\,sr}}]$	α	d_{orth} [kpc]	D_{ort} [pc]	d_{median} [kpc]	D_{median} [pc]	Δd [kpc]	ref.
1	G21.8-3.0	5.42	60.0x60.0	-21.64	-0.72	2.4	42	2.0	34	0.4	1
2	G23.11+0.18	5.67	21.7x25.0	-20.80	-0.63	4.1	28	4.0	27	0.2	2
3	G27.06+0.04	1.67	7.5x7.5	-20.35	-0.53	10.4	23	11.1	24	-0.8	3, 4
4	G28.36+0.21	2.42	6.4x6.4	-20.05	-0.28	10.6	20	12.6	23	-2.1	5, 6
5	G28.78-0.44	1.27	6.6x6.6	-20.36	-0.42	11.8	23	12.8	24	-0.9	5, 6
6	G39.4-0.0*	0.25	15.6x15.6	-21.81	-0.55	9.9	45	7.8	36	2.1	7
7	G39.5+0.4*	0.54	18.0x16.8	-21.57	-0.55	7.9	40	6.7	34	1.3	7, 4
8	G40.50+0.50	0.68	8.0x7.1	-20.74	-0.55	12.4	27	12.1	26	0.4	8
9	G42.95-0.30	1.32	2.8x2.6	-19.56	-0.55	19.9	16	27.9	22	-8.0	8
10	G46.60+0.20	0.96	8.1x7.4	-20.62	-0.55	11.4	26	11.4	26	-0.0	8
11	G47.78+2.02	0.20	3.7x2.8	-20.54	-0.55	26.4	25	26.9	25	-0.5	8
12	G51.26+0.11	14.20	11.3x11.3	-19.78	-0.40	5.3	17	6.9	23	-1.7	3, 4
13	G148.20+0.80	1.16	42.4x39.0	-21.98	-0.55	4.1	49	3.1	36	1.0	8
14	G149.10+1.90	1.25	43.4x31.3	-21.86	-0.55	4.3	46	3.3	36	1.0	8
15	G306.4+0.1*	0.12	19.2x19.2	-22.31	-0.55	10.2	57	6.7	37	3.5	7
16	G308.73+1.38	0.41	20.7x16.7	-21.75	-0.55	8.1	44	6.5	35	1.6	9
17	G309.2-0.1*	0.12	10.2x13.8	-21.89	-0.55	13.5	47	10.4	36	3.1	7
18	G310.7-5.4*	0.45	27.0x27.0	-22.03	-0.55	6.4	50	4.7	37	1.7	7
19	G312.65+2.87	0.15	5.0x4.8	-21.03	-0.55	21.8	31	20.1	29	1.7	10
20	G317.6+0.9*	0.78	34.8x26.4	-21.89	-0.55	5.3	47	4.1	36	1.2	6
21	G321.3-3.9	2.52	102.0x66.0	-22.25	-0.80	2.3	55	1.6	37	0.8	7, 11
22	G324.1+0.0	0.65	10.2x7.2	-20.88	-0.60	11.6	29	11.0	27	0.6	7
23	G329.9-0.5	0.14	1.2x1.2	-19.81	-0.49	51.9	18	67.7	23	-15.9	12
24	G332.8-1.5*	0.14	11.4x11.4	-21.79	-0.55	13.4	45	10.7	35	2.8	7
25	G333.5+0.0*	1.40	10.8x14.4	-20.87	-0.55	8.0	29	7.5	27	0.4	7
26	G335.7+0.9*	0.12	12.6x12.6	-21.94	-0.55	13.1	48	9.9	36	3.2	7
27	G336.8-0.6	0.66	10.8x16.8	-21.26	-0.60	8.9	35	7.9	31	1.0	7

Notes: * partial-shell SNRs; .

References: (1) Gao et al. (2020); (2) Maxted et al. (2019); (3) Dokara et al. (2018); (4) Dokara et al. (2021); (5) Luo et al. (2024); (6) Dokara et al. (2023); (7) Mantovanini et al. (2025); (8) Tsalapatas et al. (2024); (9) Lazarević et al. (2024); (10) Smeaton et al. (2024a); (11) Mantovanini et al. (2024); (12) Smeaton et al. (2024b).

Future research should take into account that SNRs reaching higher density ISM areas as they expand should have different evolutionary paths in the $\Sigma - D$ plane, than the SNRs expanding in a uniform density ISM.

Acknowledgements – We would like to thank the referee for the valuable comments and suggestions that improved the quality of this paper. MA and DU are supported by the Ministry of Science, Technological Development and Innovation of the Republic of Serbia, through contract no. 451-03-136/2025-03/200104. NM and BV are supported by the Ministry of Science, Technological Development and Innovation of the Republic of Serbia, through contract no. 451-03-136/2025-03/200002 with the Astronomical Observatory (Belgrade). MA and DU are also supported through the joint project of the Serbian Academy of Sciences and Arts and Bulgarian Academy of Sciences - "Search for optical counterparts to Galactic and extragalactic supernova remnants".

REFERENCES

Alarie, A., Bilodeau, A. and Drissen, L. 2014, MNRAS, 441, 2996
Allen, G. E., Chow, K., DeLaney, T., et al. 2015, ApJ, 798, 82
Ambrocio-Cruz, P., Rosado, M., Le Coarer, E., Bernal, A. and Gutiérrez, L. 2014, RMxAA, 50, 323
Andersen, M., Rho, J., Reach, W. T., Hewitt, J. W. and Bernard, J. P. 2011, ApJ, 742, 7
Arbutina, B. and Urošević, D. 2005, MNRAS, 360, 76
Berkhuijsen, E. M. 1986, A&A, 166, 257
Beuther, H., Bihr, S., Rugel, M., et al. 2016, A&A, 595, A32
Booth, R. A., Kothes, R., Landecker, T., et al. 2022, ApJ, 941, 17
Case, G. L. and Bhattacharya, D. 1998, ApJ, 504, 761
Caswell, J. L., McClure-Griffiths, N. M. and Cheung, M. C. M. 2004, MNRAS, 352, 1405
Chen, X., Wang, S. and Chen, X. 2025, ApJ, 988, 176
Combi, J. A., Benaglia, P., Romero, G. E. and Sugizaki, M. 2005, A&A, 431, L9
Dinçel, B., Neuhäuser, R., Yerli, S. K., et al. 2015, MNRAS, 448, 3196
Dokara, R., Roy, N., Beuther, H., et al. 2018, ApJ, 866, 61
Dokara, R., Brunthaler, A., Menten, K. M., et al. 2021, A&A, 651, A86
Dokara, R., Gong, Y., Reich, W., et al. 2023, A&A, 671, A145
Doroshenko, V., Pühlhofer, G. and Santangelo, A. 2023, A&A, 679, A152
Duin. 1976, IEEE Transactions on Computers, C-25, 1175
Eppens, L. K., Reynoso, E. M., Lazendic-Galloway, J., Combi, J. A. and Albacete-Colombo, J. F. 2020, MNRAS, 493, 3947
Ferrand, G. and Safi-Harb, S. 2012, AdSpR, 49, 1313
Fesen, R. A., Weil, K. E., Cisneros, I., Blair, W. P. and Raymond, J. C. 2021, MNRAS, 507, 244
Filipović, M. D., Lazarević, S., Araya, M., et al. 2024, PASA, 41, e112
Foster, T. J., Cooper, B., Reich, W., Kothes, R. and West, J. 2013, A&A, 549, A107
Frail, D. A., Goss, W. M., Reynoso, E. M., et al. 1996, AJ, 111, 1651
Gaensler, B. M., Manchester, R. N. and Green, A. J. 1998, MNRAS, 296, 813
Gao, X. Y., Reich, P., Reich, W., Hou, L. G. and Han, J. L. 2020, MNRAS, 493, 2188
Giacani, E., Smith, M. J. S., Dubner, G., et al. 2009, A&A, 507, 841
Giacani, E. B., Dubner, G. M., Green, A. J., Goss, W. M. and Gaensler, B. M. 2000, AJ, 119, 281
Green, D. A. 2025, JApA, 46, 14
Halpern, J. P., Gotthelf, E. V. and Camilo, F. 2012, ApJL, 753, L14
Hayato, A., Yamaguchi, H., Tamagawa, T., et al. 2010, ApJ, 725, 894
Hewitt, J. W. and Yusef-Zadeh, F. 2009, ApJL, 694, L16
Jeong, I.-G., Koo, B.-C., Cho, W.-K., et al. 2013, ApJ, 770, 105
Katsuda, S., Tanaka, M., Morokuma, T., Fesen, R. and Milisavljevic, D. 2016, ApJ, 826, 108
Khalatyan, A., Anders, F., Chiappini, C., et al. 2024, A&A, 691, A98
Koralesky, B., Frail, D. A., Goss, W. M., Claussen, M. J. and Green, A. J. 1998, AJ, 116, 1323
Kostić, P., Arbutina, B., Vukotić, B. and Urošević, D. 2024, ApJ, 974, 236
Kothes, R. and Dougherty, S. M. 2007, A&A, 468, 993
Kothes, R., Uyanıker, B. and Reid, R. I. 2005, A&A, 444, 871
Lazarević, S., Filipović, M. D., Koribalski, B. S., et al. 2024, Research Notes of the AAS, 8, 107
Leahy, D. and Tian, W. 2006, A&A, 451, 251
Leahy, D. A. and Green, K. S. 2012, ApJ, 760, 25
Leahy, D. A. and Tian, W. W. 2007, A&A, 461, 1013
Lee, Y.-H., Koo, B.-C. and Lee, J.-J. 2020, AJ, 160, 263
Luo, T.-X., Zhou, P. and He, H.-N. 2024, AJ, 168, 42
Mantovanini, S., Becker, W., Khokhriakova, A., et al. 2024, A&A, 690, A278
Mantovanini, S., Hurley-Walker, N. and Anderson, G. 2025, PASA, 42, e021
Maxted, N. I., Filipović, M. D., Hurley-Walker, N., et al. 2019, ApJ, 885, 129
McClure-Griffiths, N. M., Green, A. J., Dickey, J. M., et al. 2001, ApJ, 551, 394
Ogbodo, C. S., Green, J. A., Dawson, J. R., et al. 2020, MNRAS, 493, 199
Pavlović, M. Z. 2017, MNRAS, 468, 1616
Pavlović, M. Z., Urošević, D., Vukotić, B., Arbutina, B. and Göker, Ü. D. 2013, ApJS, 204, 4
Pavlovic, M. Z., Dobardzic, A., Vukotic, B. and Urosevic, D. 2014, SerAJ, 189, 25
Pavlović, M. Z., Urošević, D., Arbutina, B., et al. 2018, ApJ, 852, 84

Pineault, S., Landecker, T. L., Madore, B. and Gaumont-Guay, S. 1993, AJ, 105, 1060
Ranasinghe, S. and Leahy, D. 2022, ApJ, 940, 63
Ranasinghe, S. and Leahy, D. A. 2017, ApJ, 843, 119
Ranasinghe, S. and Leahy, D. A. 2018a, MNRAS, 477, 2243
Ranasinghe, S. and Leahy, D. A. 2018b, AJ, 155, 204
Ranasinghe, S., Leahy, D. A. and Tian, W. 2018, Open Physics Journal, 4, 1
Raymond, J. C., Winkler, P. F., Blair, W. P. and Laming, J. M. 2017, ApJ, 851, 12
Reid, M. J., Menten, K. M., Brunthaler, A., et al. 2014, ApJ, 783, 130
Reynoso, E. M., Johnston, S., Green, A. J. and Koribalski, B. S. 2006, MNRAS, 369, 416
Reynoso, E. M., Cichowolski, S. and Walsh, A. J. 2017, MNRAS, 464, 3029
Saito, M. and Matsumoto, M. 2008, in Monte Carlo and Quasi-Monte Carlo Methods 2006, ed. A. Keller, S. Heinrich and H. Niederreiter (Berlin, Heidelberg: Springer Berlin Heidelberg), 607
Sánchez-Cruces, M., Rosado, M., Fuentes-Carrera, I. and Ambrocio-Cruz, P. 2018, MNRAS, 473, 1705
Sankrit, R., Raymond, J. C., Blair, W. P., et al. 2016, ApJ, 817, 36
Sano, H., Suzuki, H., Nobukawa, K. K., et al. 2021, ApJ, 923, 15
Sasaki, M., Zangrandi, F., Filipović, M., et al. 2025, A&A, 693, L15
Sawada, M., Tachibana, K., Uchida, H., et al. 2019, PASJ, 71, 61
Shan, S. S., Zhu, H., Tian, W. W., et al. 2018, ApJS, 238, 35
Shan, S.-S., Zhu, H., Tian, W.-W., et al. 2019, RAA, 19, 092
Shklovskii, I. S. 1960, AZh, 37, 256
Smeaton, Z. J., Filipović, M. D., Koribalski, B. S., et al. 2024a, Research Notes of the AAS, 8, 158
Smeaton, Z. J., Filipović, M. D., Lazarević, S., et al. 2024b, MNRAS, 534, 2918
Sofue, Y., Kohno, M. and Umemoto, T. 2021, ApJS, 253, 17
Su, H.-Q., Zhang, M.-F., Zhu, H. and Wu, D. 2017, RAA, 17, 109
Supan, L., Castelletti, G., Peters, W. M. and Kassim, N. E. 2018, A&A, 616, A98
Takata, A., Nobukawa, M., Uchida, H., et al. 2016, PASJ, 68, S3
Tian, W. W. and Leahy, D. A. 2012, MNRAS, 421, 2593
Tian, W. W. and Leahy, D. A. 2014, ApJL, 783, L2
Tian, W. W., Haverkorn, M. and Zhang, H. Y. 2007a, MNRAS, 378, 1283
Tian, W. W., Leahy, D. A. and Foster, T. J. 2007b, A&A, 465, 907
Tian, W. W., Li, Z., Leahy, D. A., et al. 2010, ApJ, 712, 790
Tsalapatas, K., Arias, M., Shimwell, T., et al. 2024, A&A, 690, A247
Urošević, D., Vukotić, B., Arbutina, B. and Sarevska, M. 2010, ApJ, 719, 950
Uyaniker, B., Kothes, R. and Brunt, C. M. 2002, ApJ, 565, 1022
Velázquez, P. F., Dubner, G. M., Goss, W. M. and Green, A. J. 2002, AJ, 124, 2145
Vink, J. 2004, ApJ, 604, 693
Vukotić, B., Ćiprijanović, A., Vučetić, M. M., Onić, D. and Urošević, D. 2019, SerAJ, 199, 23
Wang, S., Zhang, C., Jiang, B., et al. 2020, A&A, 639, A72
Winkler, P. F., Gupta, G. and Long, K. S. 2003, ApJ, 585, 324
Yar-Uyaniker, A., Uyaniker, B. and Kothes, R. 2004, ApJ, 616, 247
Yu, B., Chen, B. Q., Jiang, B. W. and Zijlstra, A. 2019, MNRAS, 488, 3129
Zhao, H., Jiang, B., Li, J., et al. 2020, ApJ, 891, 137
Zhou, P., Zhou, X., Chen, Y., et al. 2020, ApJ, 905, 99
Zhou, X., Yang, J., Fang, M., et al. 2016, ApJ, 833, 4
Zhou, X., Su, Y., Yang, J., et al. 2023, ApJS, 268, 61
Zhu, H., Tian, W. W. and Wu, D. 2015, MNRAS, 452, 3470

АЖУРИРАНА РАДИО $\Sigma - D$ РЕЛАЦИЈА И РАСТОЈАЊА ДО ЉУСКАСТИХ ГАЛАКТИЧКИХ ОСТАТАКА СУПЕРНОВИХ - IV

Д. Урошевић[1], Б. Вукотић[2], М. Анђелић[1] и Н. Младеновић[2]

[1]*Катедра за астрономију, Математички факултет, Универзитет у Београду, Студентски трг 16, 11000 Београд, Србија*

E–mail: *dejanu@math.rs*

[2]*Астрономска опсерваторија, Волгина 7, 11060 Београд 38, Србија*

УДК 523.345 : 52–421.4 : 528.8
Оригинални научни рад

У овом раду приказујемо новоиздвојени узорак од 69 остатака супернових (ОСН) изабраних за калибраторе радио $\Sigma - D$ релације на 1 GHz. Калибратори са најпоузданије одређеним даљинама су издвојени после детаљне претраге литературе. Калибрација је извршена методом "кернел" равнања издвојеног калибрационог узорка у $\Sigma - D$ равни и процедуром ортогоналног фитовања. Употребили смо добијену калибрацију за одређивање растојања до 164 Галактичких ОСН и до 27 новодетектованих ОСН/кандидата за ОСН за које нису одређена, или су лоше одређена растојања. Анализа приказана у овом раду потврђује очекивана предвиђања из наших претходних радова да је метод "кернел" равнања погоднији за одређивање даљина до ОСН него метод базиран на ортогоналном фитовању, осим за одређивање даљина до изузетно нискосјајних остатака.